

# Deuteron Photo-disintegration at High Energies

E. C. Schulte (spokesperson), R. Gilman,

C. Glashauser, X. Jiang, G. Kumbartzki, R. Ransome

*Rutgers, The State University of New Jersey*

J. R. Arrington, D. F. Geesaman, K. Hafidi, R. J. Holt (spokesperson),

D. Potterveld, P. Reimer, P. Solvignon

*Argonne National Laboratory*

D. Dutta, H. Gao

*Duke University*

J. Dunne

*Mississippi State University*

Z.-E. Meziani

*Temple University*

A. Bruell, P. Bosted, J.P. Chen, R. Ent, D. Gaskell, D. Mack, D. Meekins

*Thomas Jefferson National Accelerator Facility*

E. R. Kinney

*University of Colorado*

E. J. Beise

*University of Maryland*

July 7, 2006

# Contents

<b>1</b>	<b>Introduction</b>	<b>4</b>
<b>2</b>	<b>Physics Motivation</b>	<b>4</b>
2.1	Meson Exchange vs. QCD . . . . .	4
2.2	Available Descriptions of Deuteron Photo-disintegration . . . . .	4
2.2.1	Traditional Meson Exchange . . . . .	5
2.2.2	Asymptotic Meson Exchange (AMEC) . . . . .	6
2.2.3	Reduced Nuclear Amplitudes/Quark Exchange . . . . .	7
2.2.4	Hard Rescattering Model . . . . .	9
2.2.5	Quark Gluon String . . . . .	10
2.2.6	Perturbative Quantum Chromodynamics– Constituent Counting Rules . . . . .	10
<b>3</b>	<b>The Experiment</b>	<b>12</b>
3.1	Overview . . . . .	12
3.2	Equipment . . . . .	13
3.2.1	Beam . . . . .	13
3.2.2	Spectrometers . . . . .	13
3.2.3	Targets and Radiator . . . . .	13
3.3	Kinematics and Rate Estimates . . . . .	14
3.4	Backgrounds, Analysis, and Systematic Uncertainty . . . . .	15
3.5	Beam Time Request . . . . .	17
<b>4</b>	<b>Collaboration Responsibilities</b>	<b>18</b>
<b>5</b>	<b>Conclusion</b>	<b>19</b>

# Abstract

High-energy, exclusive deuteron photo-disintegration ( $\gamma d \rightarrow pn$ ) is an excellent laboratory for studying the transition from meson-nucleon degrees of freedom to quark-gluon degrees of freedom in nuclear reactions. Previous measurements of  $\gamma d \rightarrow pn$  up to  $\bar{E}_\gamma = 5.5$  GeV and  $\theta_{cm} = 37^\circ$  and  $53^\circ$  indicate that the invariant cross section scales in energy consistent with the constituent counting rule description. These measurements also indicate a possible threshold for the onset of this scaling behavior.

This letter of intent describes a new set of measurements feasible at Jefferson Lab with the upgraded CEBAF accelerator and new Super-High Momentum Spectrometer (SHMS) in Hall C. Using cryogenic targets and real bremsstrahlung radiators similar in design to those used in previous JLab measurements of this process, the incident photon range can be extended to 6.6 GeV for forward angles  $\theta_{cm} = 37^\circ$  and  $53^\circ$  to confirm onset of scaling at forward angles. New measurements at  $\theta_{cm} = 90^\circ$  will confirm the persistence of scaling in the highest transverse momentum setting for this reaction.

# 1 Introduction

Exploring and understanding quark effects in nuclear reactions is a challenge of nuclear physics. The transition from meson-baryon degrees of freedom to quark-gluon degrees of freedom indicates the need to include QCD in theoretical calculations of these processes. Exclusive deuteron photo-disintegration ( $\gamma d \rightarrow pn$ ) is an excellent laboratory for studying this transition. The use of real photons increases the momentum transferred to the detected nucleon 4-fold over its companion exclusive process, elastic electron-deuteron scattering [1]. Thus, it is argued, the probability that QCD effects can be seen increases in this nuclear reaction, compared to that of electron-deuteron elastic scattering. Indeed, in high-energy  $\gamma d \rightarrow pn$  the invariant cross section does appear to follow the energy dependence predicted by the constituent counting rules for high enough photon energy [2]. This letter of intent describes a new suite of measurements intended to extend the high-energy range for the  $\gamma d \rightarrow pn$  process at  $\theta_{cm} = 37^\circ, 53^\circ$ , and  $90^\circ$ . These measurements will test the persistence of the scaling behavior observed in previous JLab measurements and provide further data on the transition from non-scaling to constituent counting behavior.

## 2 Physics Motivation

### 2.1 Meson Exchange vs. QCD

Meson exchange theory is the classical technique used to describe nucleon-nucleon interactions; and has been very successful. For deuteron photo-disintegration, however, at high energy its use has become limited. Figure 1 shows the scaled invariant differential cross section,  $s^{11} \frac{d\sigma}{dt}$ , for the deuteron photo-disintegration reaction as a function of the incident photon energy. The two models of deuteron photo-disintegration presented are able to reproduce features in the data quite well up to incident photon energies of about 500 Mev. Above this, however, they begin to lose their predictive power.

Quantum chromodynamics (QCD) is a field theory approach to the strong interaction. QCD views the hadrons, baryons and mesons, as composite objects of point-like particles, quarks. Because the coupling constant for QCD,  $\alpha_s$ , is strongly dependent on momentum transfer, perturbative methods like those used in QED are only valid at large momentum transfers. QCD is expected to be able to describe nuclear interactions, like deuteron photo-disintegration; however,  $\alpha_s$  is still relatively large even at the highest energies thus far measured in deuteron photo-disintegration, perturbative approaches are not expected to be valid [10] and non-perturbative techniques are very difficult to calculate.

### 2.2 Available Descriptions of Deuteron Photo-disintegration

As described in Section 2.1 there are two basic frameworks which can be used to describe deuteron photo-disintegration. The meson exchange picture has produced very successful models up to a few hundred MeV in photon energy. Two models, one by T. S.-H. Lee and one by J. M. Laget, have attempted to describe deuteron photo-disintegration into the 1 to 2 GeV region. The Asymptotic Meson Exchange model attempts to modify the traditional meson exchange technique by employing short range deuteron wave functions to describe the

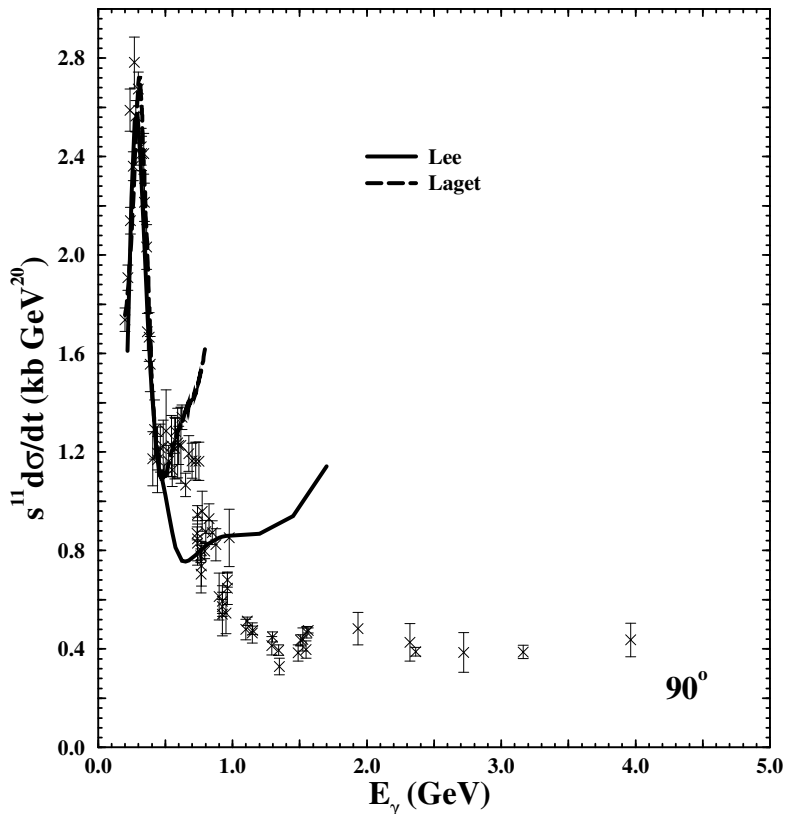


Figure 1:  $s^{11} \frac{d\sigma}{d\Omega}$  for the  $d(\gamma, p)n$  reaction up to a photon energy of 4 GeV at  $\theta_{cm} = 90^\circ$ . The solid curve is the meson exchange model developed by T.S-H. Lee [3] and the long dashed curve is the meson exchange model developed by Laget [4]. Notice that above 0.5-0.8 GeV the present models are unable to reproduce the present data. The data appear to follow an  $s^{-11}$  dependence. Data are from Refs. [5, 6, 7, 8, 9]

short distance behavior of the reaction. Models which include QCD concepts and involve single quark exchanges, such as Reduced Nuclear Amplitudes [11], a Regge model known as Quark Gluon String [12, 13, 14], and the Hard Rescattering Model [15, 16] also exist. Perturbative QCD, the high energy extreme, provides a very simple expression to predict the deuteron photo-disintegration cross section known as the Constituent Counting Rules [17]. The results for each model is displayed in Fig. 7. The following sections will summarize the important features of each of these techniques, and what they predict for the energy and angular dependencies for the differential cross section.

### 2.2.1 Traditional Meson Exchange

The meson exchange model developed by T. S.-H. Lee calculates the differential cross section for deuteron photo-disintegration only at  $90^\circ$  in the center-of-mass. This model, shown diagrammatically in Fig. 2 describes the reaction occurring in two parts involving photon absorption and subsequent nucleon-nucleon interaction. A coupled channel model for nucleon-nucleon interactions is used to characterize the final state interaction. A relativistic approach has also been taken, with little effect on the model's high energy predictive power.

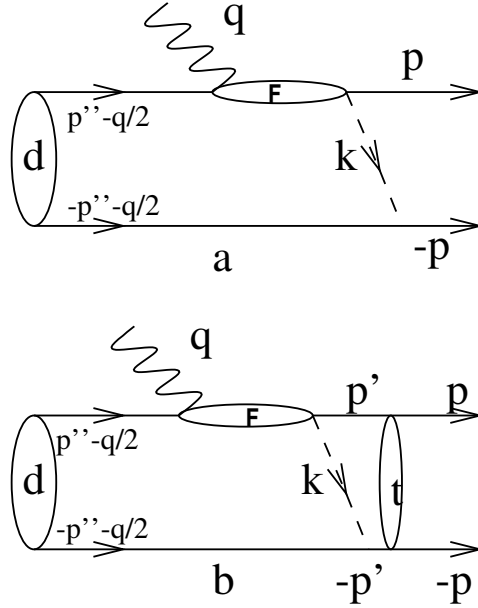


Figure 2: Diagram of Lee’s meson exchange current model. Figure a) shows the basic model being studied. Figure b) shows detail of the nucleon-nucleon final state interaction described in the model. The “bubble” in b) represents the half-off shell  $t$ -matrix governing the final state nucleon-nucleon interaction [3].

J. M. Laget also developed a meson exchange current model of deuteron photo-disintegration. This model, also only calculated the cross section at  $90^\circ$  in the center of mass, expands the cross section in terms of leading amplitudes. As shown in Fig. 1, the results of this calculation indicate good agreement up to a photon energy of approximately 0.7 GeV, after which the description begins to break down. In this model the photon is allowed to couple explicitly to the exchanged meson, which can be either a  $\rho$  or  $\pi$ . Form factors are used to reproduce the correct cross section values.

### 2.2.2 Asymptotic Meson Exchange (AMEC)

Nagorny, Dieperink, and their collaborators have devised a model [18] which attempts to extend the meson exchange concept into the few GeV photon energy region. They argue that it is not surprising that traditional meson exchange models are unsuccessful because of the short distances over which the reaction occurs. In Asymptotic Meson Exchange the short distance part of the interaction is parametrized with a strong form factor. Because the hard part of the reaction occurs over short distances, relativistic prescriptions are taken. Asymptotic Meson Exchange gives mixed results in describing the energy dependence at all energies, and angles.

The primary diagrams contributing to this model are shown in Figure 3. The short distance behavior, or “hard” part, of the process is described by a strong form factor of the following type:

$$G(p^2) = \frac{C}{(\Lambda^2/2 + m^2 - p^2)^g}. \quad (1)$$

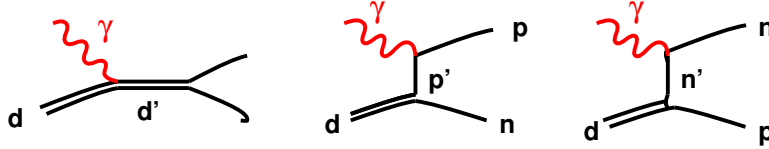


Figure 3: Asymptotic Meson Exchange Mode (AMEC) diagrams [18].

Form factors of this type are obtained from constraining the form factor to reproduce the asymptotic behavior of the basis model [19]. In Eq. 1,  $C$  is a normalization constant,  $\Lambda$  is a “range parameter,”  $m$  is the nucleon mass, and  $p$  the momentum of the off-shell nucleon [18]. Nagorny, *et al.* have used  $g = 3$  to describe the data between 1 GeV and 4 GeV photon energies [18].

Relativistic effects are important at short distances. As a result the authors transformed their prescription into light-front and instant form relativistic prescriptions. In these prescriptions the form factor is transformed into the appropriate coordinate systems.

### 2.2.3 Reduced Nuclear Amplitudes/Quark Exchange

Reduced Nuclear Amplitudes (RNA) developed by Brodsky and Hiller and Quark Exchange, developed by Radyushkin, are related methods to describe the deuteron photo-disintegration differential cross section. This method is based upon the reduced form factor technique developed by Brodsky and Chertok. In the reduced amplitude technique the transverse momentum,  $P_T$ , is the kinematic quantity which governs the onset of asymptotic scaling. The formalism devised by Radyushkin clearly illustrates the symmetric nature of the angular distribution predicted by this technique.

Brodsky and Chertok developed the reduced form factor to describe the electron-deuteron elastic form factor (see Fig. 4) [11]. The reduced form factor is given by [22]

$$f_d = \frac{F_d(q^2)}{F_N^2(\frac{1}{4}q^2)}. \quad (2)$$

In Eq. 2  $F_d$  is the deuteron form factor and  $F_N^2$  is the product of two nucleon form factors. Each nucleon is assumed to carry  $\frac{1}{4}|q|^2$ , the momentum transfer squared to the deuteron. By using the reduced form factor, the nuclear structure is effectively removed.

By analogy with the electron-deuteron ( $e$ - $d$ ) elastic form factor (Fig. 4), for which scaling sets in at  $Q^2 = 1$  (GeV/c)<sup>2</sup>, any scaling behavior for deuteron photo-disintegration is argued to set in for momentum transfers, in this case  $P_T$ , of approximately 1 GeV/c. Using this assumption the scaling condition for deuteron photo-disintegration is:

$$P_T m_{\gamma d \rightarrow pn} \simeq \text{constant}; \quad P_T^2 \geq 1 \text{ (GeV/c)}^2 \quad (3)$$

The amplitude  $m_{\gamma d \rightarrow pn}$  can be factored into an energy/momentum-dependent piece and an angular-dependent piece,

$$m_{\gamma p \rightarrow pn} = P_T^{-1} f(\theta_{cm}), \quad (4)$$

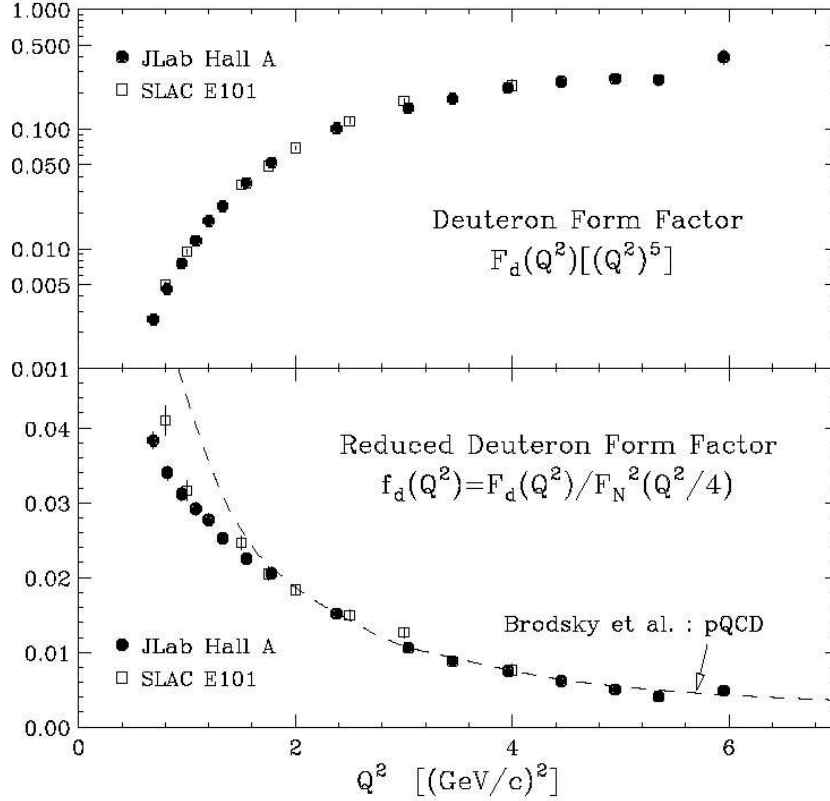


Figure 4: Electron-deuteron elastic structure function results from Jefferson Lab Hall A. The figure is from Ref. [20]. The top panel shows the deuteron form factor,  $F_d$ , multiplied by the  $Q^2$  dependence expected from pQCD predictions. The bottom panel shows the reduced form factor analysis from the RNA method. The dashed curve is the RNA prediction [21].

where  $P_T^{-1} = tu/s$  up to logarithmic terms, if particle masses are ignored [11]. From this the center of mass differential cross section can be constructed:

$$\frac{d\sigma}{d\Omega_{cm}} \sim \frac{1}{s[s - m_d^2]^{\frac{1}{2}}} \frac{F_p^2(\hat{t}_p)F_n^2(\hat{t}_n)}{P_T^2} f^2(\theta_{cm}). \quad (5)$$

Radyushkin reformulated the expression of the form factors in his Quark Exchange model. A diagram of these models can be seen in Figure 5. Radyushkin describes the amplitude in terms of energy and scattering angle in the center of mass [23]:

$$M(E, \theta_{cm}) = \frac{f^{SD}(E, \theta_{cm})}{(\mu + mE)^4} C(E, \theta_{cm}) \quad (6)$$

where  $C(E, \theta)$  is given by,

$$C(E, \theta) = \left[ 1 - \frac{\cos^2 \theta_{cm}}{(1 + \frac{m}{E})(1 + \frac{\mu^2}{mE})^2} \right]^4, \quad (7)$$

where  $\mu^2 = 0.71 \text{ GeV}^2$ ,  $E$  is the laboratory photon energy, and  $m$  is the nucleon mass. From these expressions a symmetry about  $90^\circ$  in the center of mass, given by the  $\cos^2 \theta$  term, in the angular distribution of the cross section can be seen.

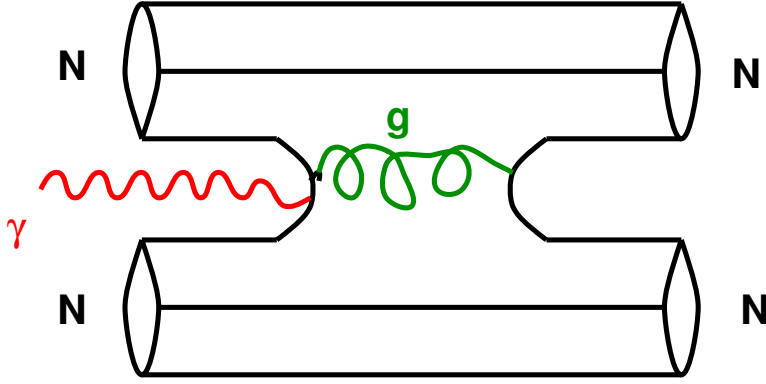


Figure 5: Quark Exchange Model [23].

### 2.2.4 Hard Rescattering Model

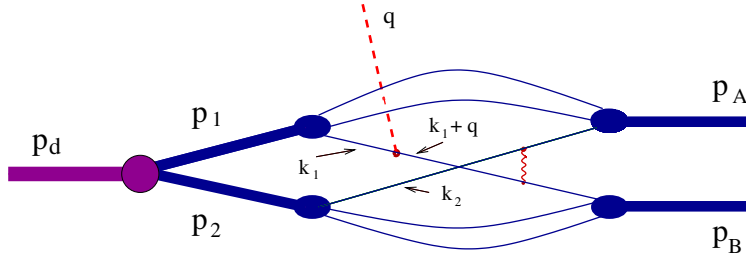


Figure 6: Hard Rescattering Model (HRM) diagram [15].

The Hard Rescattering Model, illustrated in Figure 6, allows a photon to be absorbed on a quark. This results in a high momentum scattering of the struck quark on a quark in the other nucleon. The residual nucleons have high relative momentum after the reaction [15, 16]. A low-momentum, non-relativistic deuteron wave function is used to describe the initial deuteron. The use of the low momentum wave function is necessary because the deuteron is loosely bound. The quarks which interchange in the reaction do so by exchanging a hard (high energy) gluon; and, the struck quark must not radiate any soft gluons before reaching the second quark [15, 16].

The quark interchange piece of this model is parametrized by using high energy, large angle, proton-neutron scattering data. Because little data are available at the momentum transfer per nucleon,  $t_N$ , values needed,  $\frac{d\sigma^{pn \rightarrow pn}}{dt}$ , was extrapolated to appropriate values. The proton-neutron cross section already scales as  $s^{-10}$ , so the requirement that  $\frac{d\sigma^{\gamma d \rightarrow pn}}{dt}$  scale as  $s^{-11}$  at high energies is naturally met [15, 16].

The validity of assuming that the hard quark-interchange piece can be parametrized in terms of  $np$  scattering data has been challenged. Lee and Julia-Diaz [24] have attempted a complete calculation of the quark-exchange amplitude, constrained by  $np$  scattering data. Comparing their calculation to assumptions made in the Hard Rescattering Model [15, 16], they have cast doubt on the validity of the simplifications of the HRM technique.

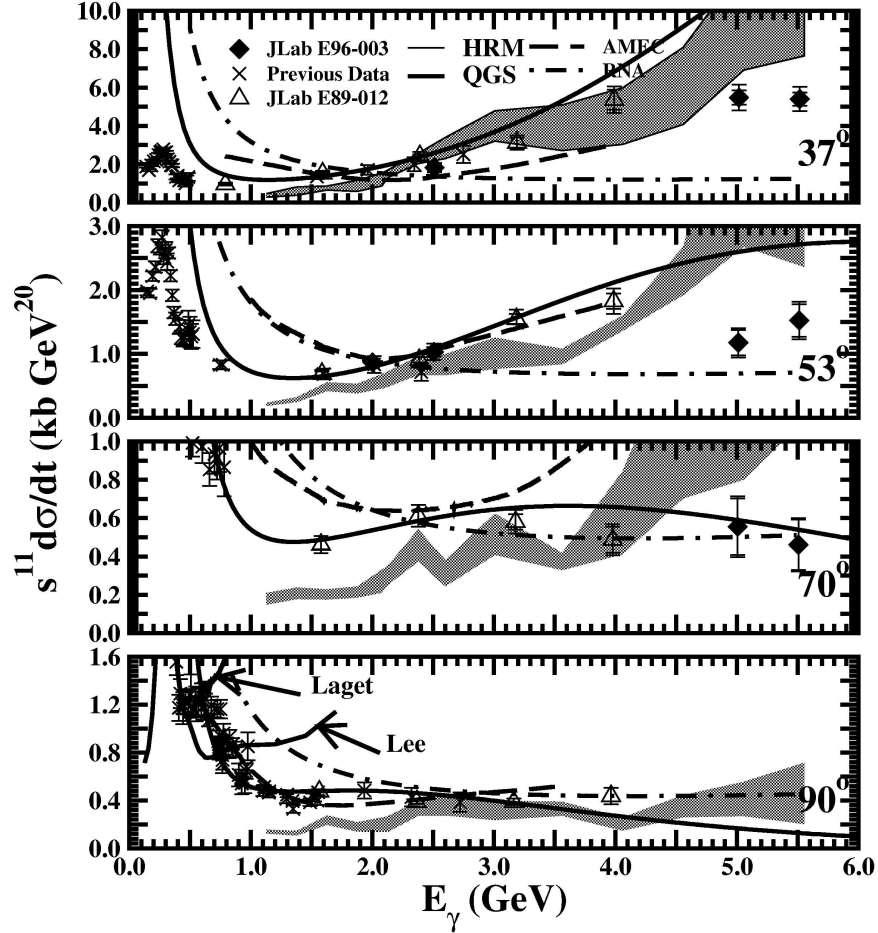


Figure 7:  $s^{11} \frac{d\sigma}{dt}$  for the  $d(\gamma, p)n$  reaction up to  $E_\gamma = 5.5$  GeV. The present data are in filled diamonds. Previous data are from references [5, 6, 7]. The curves are the various models available to calculate  $\gamma d \rightarrow pn$  as described in the text.

### 2.2.5 Quark Gluon String

The Quark Gluon String model uses Regge theory to calculate the deuteron photo-disintegration cross section. A diagram of this model is given in Fig. 8. This model uses non-linear trajectories which are derived from QCD studies following a screened quark-antiquark potential [12, 13, 14].

The quark-antiquark model was extended to baryons in order to apply the QGS to deuteron photo-disintegration. This was accomplished by describing a baryon as a composite object containing a quark and a diquark. This allows the baryon trajectories to take a similar form as the quark-antiquark systems studied in lattice QCD calculations which formed the basis for the non-linear trajectories [12, 13, 14].

### 2.2.6 Perturbative Quantum Chromodynamics— Constituent Counting Rules

Processes in quantum chromodynamics are most simply calculated in energy or distance scales where perturbative methods can be applied akin to their application in Quantum Elec-

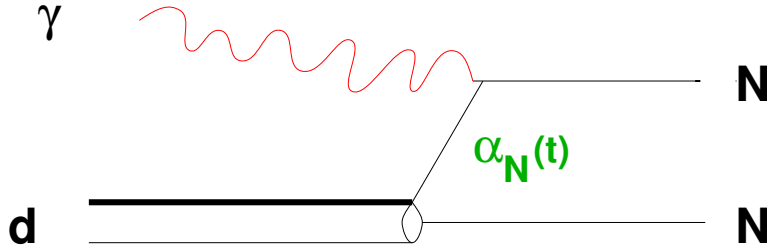


Figure 8: Quark Gluon String (QGS) Regge diagram [12].

trodynamics. The nature of the running coupling constant,  $\alpha_s(Q^2)$ , requires high energies for perturbation theory to be valid. At perturbative energy scales, however, a simple prescription exists to predict the behavior of invariant differential cross sections. Behavior consistent with these rules, known as Constituent Counting Rules, has been seen in high-energy hadronic processes. Brodsky and Lepage argue that because the QCD cutoff is between 100 MeV and 300 MeV, from experiment, pQCD could be valid for hadronic distances as large as 1 fm [17]. Using this argument it may be possible to apply a pQCD method to describe medium as well as high energy processes.

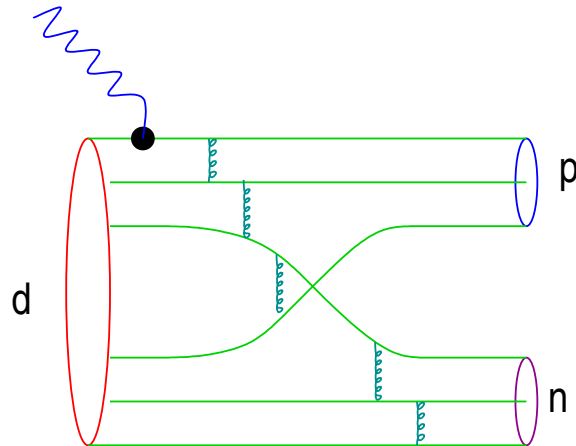


Figure 9: pQCD Feynman diagram for deuteron photo-disintegration.

The Constituent Counting Rules, sometimes called dimensional scaling laws, were developed by Matveev, Muradyan, and Tavkhelidze and Brodsky and Lepage independently. A diagram describing the pQCD process for deuteron photo-disintegration is shown in Fig. 9. The Constituent Counting Rule postulates that [17, 25]: There exists a power law scaling (constituent counting rules) for fixed angle binary reactions, i.e.  $A + B \rightarrow C + D$ :

$$\frac{d\sigma}{dt}(AB \rightarrow CD) \sim \frac{1}{s^{n-2}} f(\theta_{cm}). \quad (8)$$

The energy dependence involves only the number of constituents, or elementary fields, involved in the reaction. Elementary fields are leptons, photons, and quarks. Only those components in the initial and final states are counted. For  $\gamma d \rightarrow pn$  the constituent counting rule predicts an  $s^{-11}$  energy dependence.

Such power law scaling has been seen in hadronic reactions [26]. For example for  $s \geq 15 \text{ GeV}^2$  in proton-proton elastic scattering  $s^{-10}$  scaling is seen (see Fig. 10) [27]. Below  $s \simeq 15 \text{ GeV}^2$ , however, the power law scaling is not apparent [27].

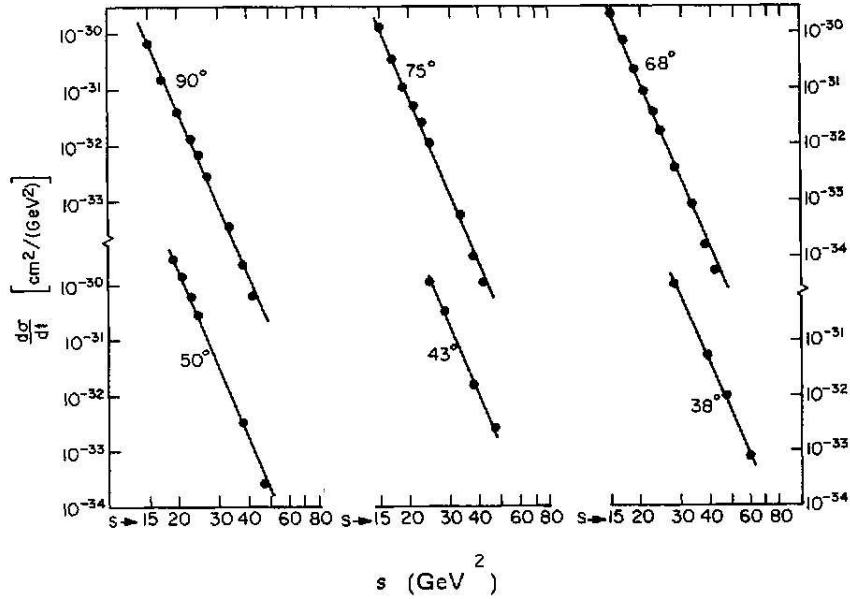


Figure 10:  $\frac{d\sigma}{dt} \sim s^{-9.7 \pm 0.4}$  seen in proton-proton elastic scattering. Data are as compiled in Ref. [27].

## 3 The Experiment

### 3.1 Overview

The high momentum transfer per nucleon in deuteron photo-disintegration [1] makes it an excellent candidate for studies of quark effects in nuclear reactions. Previous measurements completed, in Hall C at Jefferson Lab up to  $E_\gamma = 5.5 \text{ GeV}$  [28, 2] and reinforced by measurements made in Hall B [29, 30, 31], indicate that the onset of scaling behavior consistent with the constituent counting rules [2] becomes observable at a transverse momentum of  $p_T \approx 1.3 \text{ GeV}/c$ . Using the upgraded high-energy, continuous wave electron beam, from CEBAF, further measurements can be readily made.

These new measurements, up to  $E_\gamma = 6.6 \text{ GeV}$  will be able to confirm the persistence of the  $s^{-11}$  scaling behavior in the  $\gamma d \rightarrow pn$  reaction. By continuing the data set at  $\theta_{cm} = 37^\circ, 53^\circ$ , and  $90^\circ$  a detailed study can be performed in the energy range where the apparent transition takes place. This will improve the estimate of the transverse momentum,  $p_T$ , at which scaling begins, and add important empirical measurements needed for improved theoretical studies of this transition.

## 3.2 Equipment

### 3.2.1 Beam

This measurement will use the upgraded high energy electron beam from CEBAF. The energies requested range from 2.268 to 6.668 GeV in 1.1 GeV increments (1/2 pass steps) at 30  $\mu$ A. These energies will provide data which overlaps with previous measurements, important for cross-checking both new equipment (SHMS) and the virtual photon analysis technique needed to make these measurements in reasonable time (see Sec. 3.4).

### 3.2.2 Spectrometers

Detection of the photo-protons from the  $\gamma d \rightarrow pn$  reaction will be done with the Super-High Momentum Spectrometer (SHMS) for  $\theta_{cm} = 37^\circ$  and  $53^\circ$  and the High Momentum Spectrometer (HMS) for  $\theta_{cm} = 70^\circ$  and  $90^\circ$ . The pertinent details of these spectrometers are given in Table 1. These spectrometers with their high central momenta, ability to achieve small angles, and modest solid angles make Hall C the appropriate experimental hall for these measurements. In both spectrometers a Cerenkov detector with 1 atm of  $C_4F_{10}$ , or other appropriate gas/pressure combination will be required for high momentum ( $> 2.5$  GeV/ $c$ ) pion rejection.

HMS and SHMS Technical Specifications		
	HMS	SHMS
Spectrometer Type	QQQD	QQQD
Maximum Central Momentum	7.4 GeV/ $c$	11 GeV/ $c$
Angle Ranges	$23^\circ$ to $\sim 90^\circ$	$5.5^\circ$ to $25^\circ$
Momentum Resolution	$<0.1\%$	$\sim 0.12\%$
Momentum Acceptance	$\pm 18\%$	$-15\%$ to $+20\%$
Solid Angle, extended target	$\sim 6$ msr	$\sim 3.5$ msr

Table 1: Technical specifications for the HMS and SHMS. The SHMS will be new equipment in Hall C. Note that the minimum angle between the HMS and SHMS is  $17.5^\circ$

### 3.2.3 Targets and Radiator

This experiment will need the 15 cm Hall C cryogenic targets filled with liquid deuterium and hydrogen. The liquid hydrogen will be used to assess backgrounds. These are approximately a 2% radiation length target for these cryogens.

Heat loads and target boiling are always a concern when working with cryogenic targets, both for the data quality and target safety. At the requested current of  $30\mu$ A, the targets will dissipate approximately 150 watts, well within the acceptable range for 500 W targets such as those used in Hall C for JLab E89-012 and E96-003. Expected luminosity for a 15 cm target at this current is  $\sim 1.4 \times 10^{38}/\text{cm}^2/\text{s}$ . Previous experience from JLab E89-012

and E96-003 indicates that cryo-targets of the design used in these experiments tolerate such luminosities well.

These  $\gamma d \rightarrow pn$  measurements will use real photons produced by bremsstrahlung. The photons will be produced using a 6% radiation length copper radiator as in previous Hall C measurements. This will be installed approximately 1 meter upstream of the target such that it is not visible by the SHMS at the most forward angles. The radiator at 30  $\mu\text{A}$  will be required to dissipate approximately 75 watts, well tolerated by a radiator of the design used in JLab E96-003.

### 3.3 Kinematics and Rate Estimates

Table 2 shows the mean photon energies, beam energies, laboratory angles, and central spectrometer momenta needed for this measurement. Notice that the  $\theta_{cm} = 37^\circ$  and  $53^\circ$  degree measurements will be taken with the SHMS and the  $\theta_{cm} = 70^\circ$  and  $90^\circ$  with the HMS. For both spectrometers, the settings are well within the angle and momentum ranges specified (see Table 1). For the remaining two lower-energy  $\theta_{cm} = 70^\circ$  measurements the SHMS will have to be moved such that the HMS can be positioned to take data.

<b>Kinematic Settings: Beam and Spectrometer</b>					
$E_\gamma$ (GeV)	$E_{beam}$ (GeV)	$\theta_{cm}(\circ)$	$\theta_{lab}(\circ)$	$P_{lab}$ (GeV)	Spectrometer
2.2	2.268	37	19.16	2.673	SHMS
2.2	2.268	53	28.09	2.473	SHMS
2.2	2.268	70	38.39	2.206	HMS
2.2	2.268	90	52.13	1.847	HMS
3.3	3.368	37	16.83	3.693	SHMS
3.3	3.368	53	24.75	3.39	SHMS
3.3	3.368	70	33.99	2.987	HMS
3.3	3.368	90	46.54	2.448	HMS
4.4	4.468	37	15.19	4.7	SHMS
4.4	4.468	53	22.39	4.292	SHMS
4.4	4.468	90	42.5	3.029	HMS
5.5	5.567	37	13.96	5.701	SHMS
5.5	5.567	53	20.6	5.187	SHMS
5.5	5.567	90	39.38	3.601	HMS
6.6	6.667	37	12.98	6.699	SHMS
6.6	6.667	53	19.18	6.078	SHMS
6.6	6.667	90	36.87	4.167	HMS

Table 2: Kinematic settings for each proposed point.

Table 5 lists the rates and time needed for each target and radiator configuration at each energy and center-of-mass angle. The rate were calculated using a 6% radiator and the constituent counting rule  $s^{-11}$  energy dependence observed in JLab E96-003 [2]. The required statistical precision are summarized in Table 3. This will give good test of between continuation of the  $s^{-11}$  scaling behavior. Also included in the rate estimates are estimates for

Statistical Precisions				
$E_\gamma$	37°	53°	70°	90°
2.2	0.05	0.05	0.05	0.05
3.3	0.05	0.05	0.05	0.05
4.4	0.1	0.1	—	0.15
5.5	0.1	0.1	—	0.15
6.6	0.1	0.15	—	0.2

Table 3: Statistical precisions for  $\gamma d \rightarrow pn$  up to 6.6 GeV.

Parameters used in rate calculations	
Cross Section	$s^{11} \frac{d\sigma}{dt}$
beam current	30 $\mu A$
Radiator Thickness (radiation lengths)	6% Cu
Target Thickness (cm)	15
(radiation lengths)	2%
HMS Solid Angle (mSr)	6
SHMS Solid Angle (mSr)	3.5
Background	40%
Computer Live Time	0.8
Proton Transmission	0.9
Tracking Efficiency	0.95

Table 4: Parameters used to calculate rates for  $\gamma d \rightarrow pn$  up to  $\bar{E}_\gamma = 6.6$  GeV

computer live time, proton transmission through the spectrometers, and tracking efficiency. These parameters are summarized in Table 4.

### 3.4 Backgrounds, Analysis, and Systematic Uncertainty

Backgrounds for  $\gamma d \rightarrow pn$  are attributed to two-step processes from the aluminum target components (windows, flow diverters, etc.). These processes can produce protons which appear above the bremsstrahlung end-point in reconstructed  $E_\gamma$  spectra. The liquid hydrogen target is used to determine the shape of this background.

Analysis of the background-to-signal ratio from the high energy  $\gamma d \rightarrow pn$  data taken during JLab E96-003 allows for an extrapolation of the background rates as the energy increases. For the worst background case, at  $\theta_{cm} = 37^\circ$  at  $\bar{E}_\gamma = 5.5$  GeV, the background was approximately 35% of the measured signal. This ratio decreases with increasing center-of-mass angles. For example at  $\theta_{cm} = 53^\circ$ , the background-to-signal ratio dropped to approximately 20% of the measured signal. At both  $\bar{E}_\gamma = 5.0$  and 5.5 GeV this ratio remained reasonably constant. Thus, it has been assumed that the backgrounds from two-step processes will remain at a reasonably constant background-to-signal ratio through 6.6 GeV, the highest energy requested.

Figure 11 shows a reconstructed photon spectrum after all geometric cuts have been

Rates and Times for $d(\gamma, p)n$ at high energy									
$E_\gamma$ (GeV)	$\theta_{cm}(\circ)$	Rates (events/min)				Time (minutes)			
		LD <sub>2</sub>		LH <sub>2</sub>		LD <sub>2</sub>		LH <sub>2</sub>	
Radiator		In	Out	In	Out	In	Out	In	Out
2.2	37	504.7	88.56	108.8	35.42	6.265	2.625	2.909	1.66
	53	133.2	23.24	28.75	9.298	23.65	9.881	10.99	6.249
	70	83.01	14.43	17.95	5.772	37.8	15.76	17.58	9.968
	90	58.23	10.07	12.61	4.027	53.65	22.31	24.97	14.11
		Rates (events/hr)				Time (hours)			
3.3	37	1479	264.5	316.9	105.8	2.171	0.9179	1.005	0.5805
	53	383.5	68.21	82.28	27.28	8.339	3.517	3.863	2.224
	70	232.8	41.23	50.02	16.49	13.69	5.761	6.345	3.644
	90	156.4	27.55	33.66	11.02	20.29	8.514	9.411	5.385
4.4	37	145.2	—	31.19	—	5.492	—	2.545	—
	53	37.2	—	8.002	—	21.35	—	9.903	—
	90	14.45	—	3.118	—	24.24	—	11.26	—
5.5	37	20.37	—	4.701	—	21.84	—	10.49	—
	53	5.177	—	1.196	—	85.72	—	41.2	—
	90	1.942	—	0.4497	—	101.1	—	48.68	—
6.6	37	4.145	—	0.9552	—	107.6	—	51.64	—
	53	1.047	—	0.2415	—	188.9	—	90.73	—
	90	0.3819	—	0.08832	—	290	—	139.5	—

Table 5: Event rates calculated for each energy and angle setting for  $\gamma d \rightarrow pn$  up to 6.6 GeV. Rates were calculated assuming the  $s^{-11}$  energy dependence observed in E96-003 and parameters summarized in Table 4.

applied. Key cuts in this analysis are the y-target cut, which eliminates the aluminum target windows, but not any internal aluminum components, and the particle identification cut. Photo-protons are identified by cutting on the reconstructed mass of particles detected by the spectrometer ( $M^2$ ). Combined with background subtraction, assessed with the hydrogen target, a clear  $E_\gamma$  reconstruction is observed (Fig. 12).

Systematic errors for this experiment are summarized in Table 6 based on experience from JLab E96-003. The largest sources of systematic error arise from the target cut removing the aluminum target windows (4.5%) and the effect of the residual electron beam through the virtual photon technique [32] (5% to 9%). This will be discussed further below. Other important systematic effects are the beam current measurement and solid angle determinations.

## Virtual Photon Method

To keep the time needed to complete these measurements under control, the highest energy measurements will acquire all data with the radiator in. This prohibits a direct assessment of the effect of the residual electron beam. Accounting for these residual electron

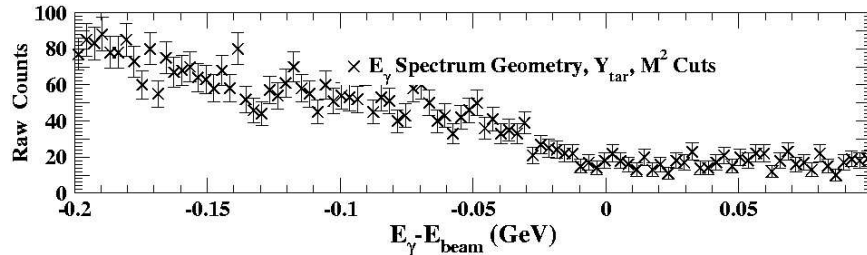


Figure 11:  $E_\gamma$  spectra for JLab Experiment E96-003 at  $E_b=5.566$  GeV at  $\theta_{cm} = 37^\circ$ . The three panels show the effects of adding analysis cuts to the data set.

E96-003 Corrections and Systematic Errors		
	Correction (%)	Error (%)
Matthews and Owens Bremsstrahlung Calculation		3
Wright and Tiator Virtual Photon Correction		5
Beam Current		1.4
Solid Angle		2.5
Particle Identification		3
Proton Attenuation	10-11	2
Tracking Efficiency	2	2
Target Cut		4.5
Background Subtraction		2

Table 6: Dominant corrections and systematic errors for Experiment E96-003, up to  $E_\gamma = 5.5$  GeV. Projected errors are expected to be very similar to those in previous measurements.

interactions will be estimated by using the virtual photon method including nuclear recoil [32]. This method related the deuteron electro-disintegration cross section to the deuteron photo-disintegration cross section. This method recently has been studied by direct measurements of the electro-disintegration and photo-disintegration cross sections at low energy (265 MeV and 365 MeV) [33]. This study found that the error from this method could be as high as 9%. Analysis of  $E_\gamma=2.0$  and 2.5 GeV data taken during E96-003 using the traditional direct subtraction method and the virtual photon method estimated the effect at about 5% for higher energies. Thus the high-precision, lower-energy data requested on all 4 target/radiator combinations is essential for estimating this error at the highest energies.

### 3.5 Beam Time Request

The beam request for these measurements is summarized in Table 3.5. This request assumes running the  $\theta_{cm} = 90^\circ$  data points in tandem with the  $\theta_{cm} = 37^\circ$  and  $53^\circ$  data points at the same energy. The  $\theta_{cm} = 70^\circ$  degree will be taken separately. Also included in the experimental time estimate is overhead at the schedule estimated in Table 8. Altogether the request is for 32.2 days of beam time plus 1.7 days of overhead. The request assumes 100% facility efficiency.

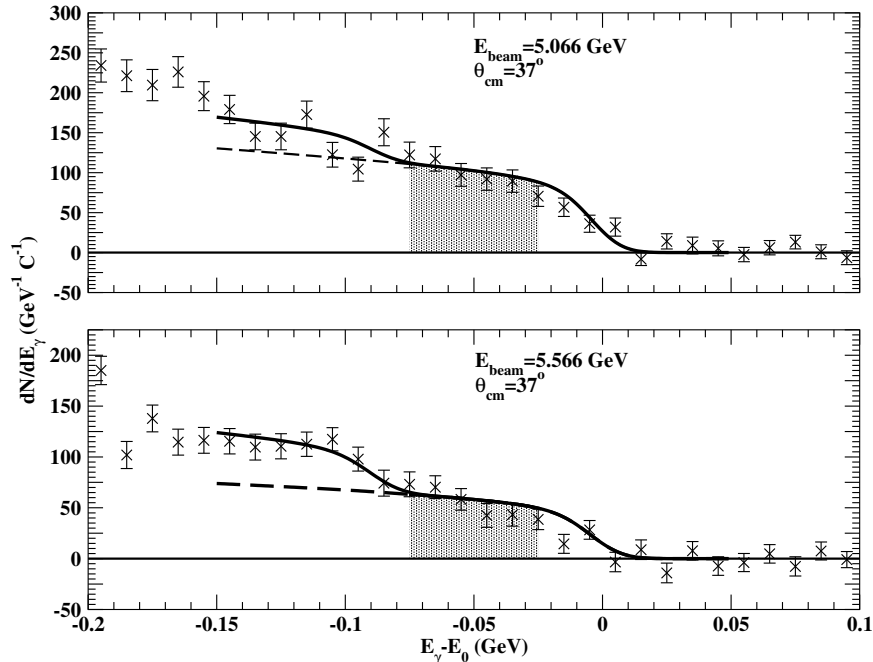


Figure 12:  $E_\gamma$  spectra for JLab Experiment E96-003 at  $E_b=5.066$  GeV at  $\theta_{cm} = 37^\circ$ , top panel, and  $E_b=5.566$  at  $\theta_{cm} = 37^\circ$ , bottom panel after cuts and background subtraction. The solid curve illustrates the clear bremsstrahlung end-points in these spectra, as well as the threshold for  $\pi^0$  production. The grey shaded area represents the region in  $E_\gamma$  used to calculate the photo-proton yield. These spectra represent data taken with the worst background conditions during E96-003.

## 4 Collaboration Responsibilities

The collaboration members are responsible for the safe and efficient taking of data during this experiment. The collaboration will provide at least one member per shift who is trained in the correct changing of the targets and radiator. The targets and radiators requested are similar in design to those previously commissioned in Hall C for earlier deuteron photo-disintegration experiments. Many members of the collaboration have participated in the previous deuteron photo-disintegration experiments at Jefferson Lab or other photo-reaction experiments elsewhere.

### Technical Responsibilities for 12 GeV Upgraded

Argonne, has the technical responsibility for the initial SHMS optics design, field maps, and optics verification of the SHMS.

Rutgers University is planning to work with Hall C and University of North Carolina on the fabrication of the new quartz hodoscope for the SHMS through funding and/or software development.

<b>Beam Time Request for <math>d(\gamma, p)n</math> at high energy</b>		
$E_\gamma$ (GeV)	$E_{beam}$	Time (days)
2.2	2.268	0.136
3.3	3.368	3.043
4.4	4.468	2.404
5.5	5.567	6.636
6.6	6.667	18.28
Total Data Request		30.5
Overhead		
Energy Changes		1.3
Target Changes		0.13
Radiator Changes		0.13
Spectrometer Changes		0.15
Total Overhead		1.7
Total Request		32.2

Table 7: Beam request for  $\gamma d \rightarrow pn$  up to 6.6 GeV. Time is measured in days for 100% facility efficiency.

## 5 Conclusion

The new data range with expected statistical precision is shown in Fig. 13. These new data will further extend the range in photon energy for the  $\gamma d \rightarrow pn$  reaction allowing the possibility to investigate the onset and persistence of the  $s^{-11}$  scaling behavior previously observed. Data taken at lower energies ( $E_\gamma=2.2$  and 3.3 GeV) will provide needed data in the transition region. These lower-energy data will also be used for the necessary cross checking of new equipment and assessment of systematic errors from the virtual photon technique at higher energies. Altogether these data will provided much needed empirical information for understanding the nature of QCD effects in exclusive nuclear reactions.

<b>Overhead Schedule</b>			
Item	Duration (hours)	Number of Occurrences	Total (hours)
Energy Change	8	4	32
Target Changes	0.25	12	3
Radiator Changes	0.167	18	3
Spectrometer Changes	0.5	7	3.5
		Total (hours)	41.5
		Total (days)	1.7

Table 8: Overhead schedule for proposed running of  $\gamma d \rightarrow pn$  up to  $\bar{E}_\gamma = 6.6$  GeV

## Deuteron Photodisintegration

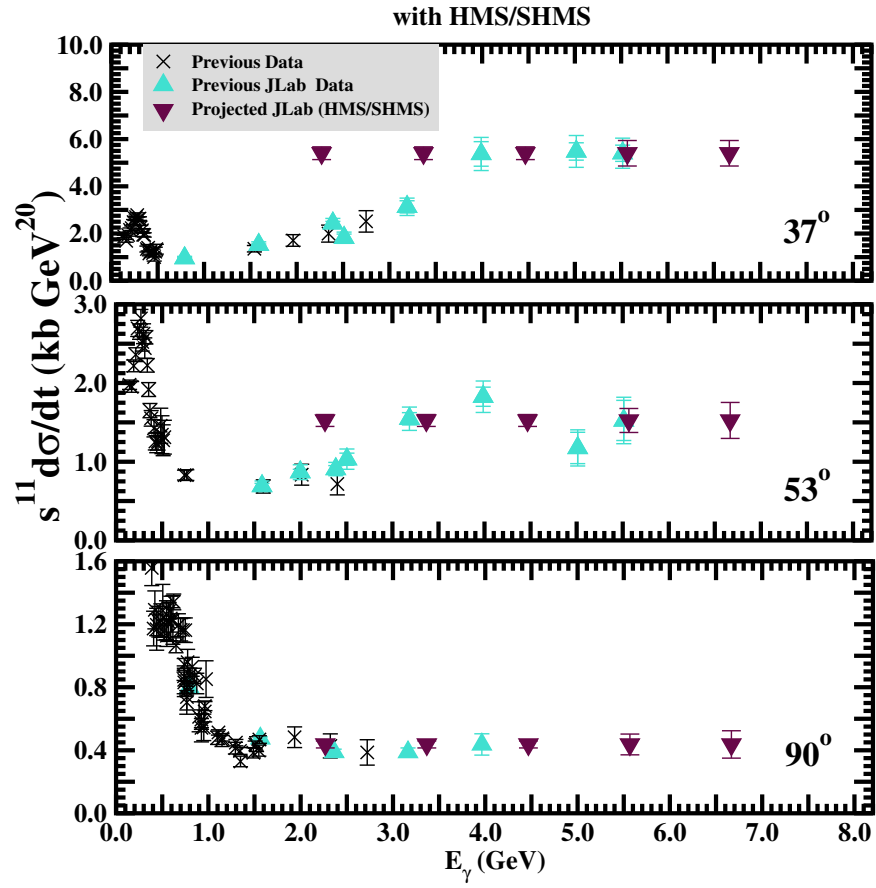


Figure 13: Expected precision for  $\gamma d \rightarrow pn$  as described in this letter of intent. Notice the overlap with previous JLab data to cross-check and verify systematic techniques.

## References

- [1] R. J. Holt. *Phys. Rev. C*, 41:2400, 1990.
- [2] E. C. Schulte et al. *Phys. Rev. Lett.*, 87:102302, 2001.
- [3] T. S.-H. Lee. In *Proceedings of the International Conference on Medium and High Energy Nuclear Physics, Taipei, Taiwan*, page 563. World Scientific, Singapore, 1988.
- [4] J. M. Laget. *Nucl. Phys.*, A312:265, 1978.
- [5] B. P. Terburg. PhD thesis, Univeristy of Illinois at Urbana-Champaign, 1999.
- [6] E. Belz. PhD thesis, California Institute of Technology, 1994.
- [7] T. Y. Tung. PhD thesis, Northwestern University, 1992.
- [8] P. Dougan et al. *Z. Phys.*, A276:55, 1976.
- [9] R. Crawford et al. *Nucl. Phys.*, A603:303, 1996.
- [10] N. Isgur and C. H. Llewellyn Smith. *Nucl. Phys.*, B317:526, 1989.
- [11] S. J. Brodsky and J. R. Hiller. *Phys. Rev. C*, 28:475, 1983.
- [12] V. Y. Grishina et al. *Eur. Phys. J.*, A10:355, 2001.
- [13] V. Y. Grishina et al. *Eur. Phys. J.*, A18:207, 2003.
- [14] V. Y. Grishina et al. *Eur. Phys. J.*, A19:117, 2004.
- [15] L. L. Frankfurt et al. *Phys. Rev. Lett.*, 84:3045, 2000.
- [16] M. M. Sargsian, 2002. nucl-th/0208027.
- [17] S. J. Brodsky and G. P. Lepage. *Nucl. Phys.*, A353:247c, 1981.
- [18] A. E. L. Dieperink and S. I. Nagorny. *Phys. Lett.*, B456:9, 1999.
- [19] F. Gross and D. B. Keister. *Phys. Rev. C*, 28:823, 1983.
- [20] L. C. Alexa et al. *Phys. Rev. Lett.*, 82:1374, 1999.
- [21] S. J. Brodsky et al. *Phys. Rev. Lett.*, 51:83, 1983.
- [22] S. J. Brodsky and B. T. Chertok. *Phys. Rev. Lett.*, 37:269, 1976.
- [23] A. V. Radushkin, 1999. JLAB-THY-99-Draft.
- [24] B. Julia-Diaz and T.-S. H. Lee. *Mod. Phys. Lett. A*, 18:200, 2003.
- [25] V. A. Matveev et al. *Lett. Nuovo Cim.*, 7:719, 1973.
- [26] C. White et al. *Phys. Rev. D*, 49:58, 1994.

- [27] V. P. Landshoff and J. C. Polkinghorn. *Phys. Lett.*, 44B:293, 1973.
- [28] C. W. Bochna et al. *Phys. Rev. Lett.*, 81:4576, 1998.
- [29] P. Rossi et al. *Phys. Rev. Lett.*, 94:012301, 2005.
- [30] P. Rossi. *Eur. Phys. J.*, A17:433, 2003.
- [31] M. Mirazita et al. *Phys. Rev. C*, 70:014005, 2004.
- [32] L. E. Wright and L. Tiator. *Phys. Rev. C*, 26:2349, 1982.
- [33] M. Yuly et al. *Phys. Rev. C*, 68:014601, 2003.

## List of Figures

1	$s^{11} \frac{d\sigma}{d\Omega}$ for the $d(\gamma, p)n$ reaction up to a photon energy of 4 GeV at $\theta_{cm} = 90^\circ$ . The the solid curve is the meson exchange model developed by T.S-H. Lee [3] and the long dashed curve is the meson exchange model developed by Laget [4]. Notice that above 0.5-0.8 GeV the present models are unable to reproduce the present data. The data appear to follow an $s^{-11}$ dependence. Data are from Refs. [5, 6, 7, 8, 9] . . . . .	5
2	Diagram of Lee's meson exchange current model. Figure a) shows the basic model being studied. Figure b) shows detail of the nucleon-nucleon final state interaction described in the model. The "bubble" in b) represents the half-off shell $t$ -matrix governing the final state nucleon-nucleon interaction [3]. . . . .	6
3	Asymptotic Meson Exchange Mode (AMEC) diagrams [18]. . . . .	7
4	Electron-deuteron elastic structure function results from Jefferson Lab Hall A. The figure is from Ref. [20]. The top panel shows the deuteron form factor, $F_d$ , multiplied by the $Q^2$ dependence expected from pQCD predictions. The bottom panel shows the reduced form factor analysis from the RNA method. The dashed curve is the RNA prediction [21]. . . . .	8
5	Quark Exchange Model [23]. . . . .	9
6	Hard Rescattering Model (HRM) diagram [15]. . . . .	9
7	$s^{11} \frac{d\sigma}{d\Omega}$ for the $d(\gamma, p)n$ reaction up to $E_\gamma=5.5$ GeV. The present data are in filled diamonds. Previous data are from references [5, 6, 7]. The curves are the various models available to calculate $\gamma d \rightarrow pn$ as described in the text. . . . .	10
8	Quark Gluon String (QGS) Regge diagram [12]. . . . .	11
9	pQCD Feynman diagram for deuteron photo-disintegration. . . . .	11
10	$\frac{d\sigma}{dt} \sim s^{-9.7 \pm 0.4}$ seen in proton-proton elastic scattering. Data are as compiled in Ref. [27]. . . . .	12
11	$E_\gamma$ spectra for JLab Experiment E96-003 at $E_b=5.566$ GeV at $\theta_{cm} = 37^\circ$ . The three panels show the effects of adding analysis cuts to the data set. . . . .	17

12	$E_\gamma$ spectra for JLab Experiment E96-003 at $E_b=5.066$ GeV at $\theta_{cm} = 37^\circ$ , top panel, and $E_b=5.566$ at $\theta_{cm} = 37^\circ$ , bottom panel after cuts and background subtraction. The solid curve illustrates the clear bremsstrahlung end-points in these spectra, as well as the threshold for $\pi^0$ production. The grey shaded area represents the region in $E_\gamma$ used to calculate the photo-proton yield. These spectra represent data taken with the worst background conditions during E96-003. . . . .	18
13	Expected precision for $\gamma d \rightarrow pn$ as described in this letter of intent. Notice the overlap with previous JLab data to cross-check and verify systematic techniques. . . . .	20

## List of Tables

1	Technical specifications for the HMS and SHMS. The SHMS will be new equipment in Hall C. Note that the minimum angle between the HMS and SHMS is $17.5^\circ$ . . . . .	13
2	Kinematic settings for each proposed point. . . . .	14
3	Statistical precisions for $\gamma d \rightarrow pn$ up to 6.6 GeV. . . . .	15
4	Parameters used to calculate rates for $\gamma d \rightarrow pn$ up to $\bar{E}_\gamma = 6.6$ GeV . . . . .	15
5	Event rates calculated for each energy and angle setting for $\gamma d \rightarrow pn$ up to 6.6 GeV. Rates were calculated assuming the $s^{-11}$ energy dependence observed in E96-003 and parameters summarized in Table 4. . . . .	16
6	Dominant corrections and systematic errors for Experiment E96-003, up to $E_\gamma = 5.5$ GeV. Projected errors are expected to be very similar to those in previous measurements. . . . .	17
7	Beam request for $\gamma d \rightarrow pn$ up to 6.6 GeV. Time is measured in days for 100% facility efficiency. . . . .	19
8	Overhead schedule for proposed running of $\gamma d \rightarrow pn$ up to $\bar{E}_\gamma = 6.6$ GeV . . . . .	19